VIP Energy Conversion Very Important Paper

DOI: 10.1002/anie.201409422

Transparent Metal Selenide Alloy Counter Electrodes for High-Efficiency Bifacial Dye-Sensitized Solar Cells**

Yanyan Duan, Qunwei Tang, Juan Liu, Benlin He, and Liangmin Yu**

Abstract: *The exploration of cost-effective and transparent counter electrodes (CEs) is a persistent objective in the development of bifacial dye-sensitized solar cells (DSSCs). Transparent counter electrodes based on binary-alloy metal selenides (M-Se; M = Co, Ni, Cu, Fe, Ru) are now obtained by a mild, solution-based method and employed in efficient bifacial DSSCs. Owing to superior charge-transfer ability for the I^-/I_3^- redox couple, electrocatalytic activity toward I_3^- reduction, and optical transparency, the bifacial DSSCs with CEs consisting of a metal selenide alloy yield front and rear efficiencies of 8.30 % and 4.63 % for $Co_{0.85}Se$, 7.85 % and 4.37 % for $Ni_{0.85}Se$, 6.43 % and 4.24 % for $Cu_{0.50}Se$, 7.64 % and 5.05 % for FeSe, and 9.22 % and 5.90 % for $Ru_{0.33}Se$ in comparison with 6.18 % and 3.56 % for a cell with an electrode based on pristine platinum, respectively. Moreover, fast activity onset, high multiple start/stop capability, and relatively good stability demonstrate that these new electrodes should find applications in solar panels.*

Dye-sensitized solar cells (DSSCs),[1–4] a class of photoelectrochemical devices that directly convert solar energy into electricity with no emission, are one of the promising alternatives for silicon solar cells. They have attracted tremendous scientific and industrial interest in the past two decades because of their simple fabrication process, environmental friendliness, and advances in technical aspects. Since the first prototype, which was reported by O'Regan and Grätzel in 1991,[5] great achievements have been made on DSSCs.[6–9] However, their commercialization is still premature. Until now, one of the most limiting impasses in the development of commercial DSSCs is their cost.[10] Owing to the historically high price for platinum feedstock, a traditional counter electrode (CE) material, a cell cannot be fabricated at a cost that is low enough to compete with conventional silicon solar cells.

Although carbonaceous materials,[11,12] conducting polymers,[13,14] or their combinations have been proposed as alternative CE materials to replace Pt in DSSCs, their poor long-term stabilities and electrocatalytic activities often render them unsuitable.[15] Moreover, inorganic compounds such as metal sulfides, nitrides, and carbides, have received attention as cost-effective and scalable photovoltaic materials,[16,17] but they suffer from unsatisfactory power conversion efficiencies when employed in DSSC devices. Recently, the emerging concept of bifacial illumination was introduced by Grätzel and co-workers, which should help to reduce the cost of solar to electric energy conversion.[18] A bifacial DSSC collects sunlight from either of its two sides, facilitating practical applications.[19] Although the known bifacial DSSCs realize electricity generation from either a photoanode or a CE, effective bifacial operation requires fine tuning of a number of parameters.[20] Independent of whether transparent carbonaceous materials, conducting polymers, metal sulfides, or metallic Pt CEs are used for bifacial DSSCs, they always suffer from modest rear efficiency and unsatisfactory stability. Additionally, owing to the metallic luster, the strong reflection of the incident light by the Pt electrode also weakens electron generation; therefore, transparent, or at least semitransparent, CEs appear to be crucial in achieving high efficiency for rear illumination. As part of our research on designing bifacial DSSCs, we are impelled to develop cost-effective, transparent, robust, scalable, and solution-processable CE materials. Herein, we propose a mild solution-based strategy for the synthesis of transparent M-Se (M = Co, Ni, Cu, Fe, Ru) binary alloy CEs. When selecting alternative metals their electronic structure is particularly relevant. The mentioned metals are all typical transition metals with a partially filled d orbital. Therefore, the alloying of these metals with Se may accept electrons to form coordinated intermediates, which is a prerequisite for robust CE materials. Although Ru is a precious metal, the low Ru dosage makes its alloy system a cost-effective CE material. Alloy materials have been established as robust electrocatalysts for energy nanodevices. When a transparent alloy CE is used in a bifacial DSSC, the incident light can easily penetrate the CE for dye excitation, which leads to a significant enhancement in rear efficiency and a reduction in the cost of solar energy conversion. The incident light (simulated air mass 1.5 global sunlight (AM 1.5), calibrated with a standard silicon solar cell) from a solar simulator can irradiate the solar cell from either the front or the rear side for electricity generation (see the Supporting Information, Figure S1). Our system shows

[*] Y. Duan, Prof. Q. Tang, J. Liu, Dr. B. He, Prof. L. Yu
Key Laboratory of Marine Chemistry and Technology, Ministry of Education, Ocean University of China and Institute of Materials Science and Engineering, Ocean University of China
238 Songling Road, Laoshan District, Qingdao 266100 (P.R. China)
E-mail: tangqunwei@ouc.edu.cn
yuyan@ouc.edu.cn

[**] We acknowledge financial support from the Fundamental Research Funds for the Central Universities (201313001, 201312005), the Shandong Province Outstanding Youth Scientist Foundation Plan (BS2013CL015), the Shandong Provincial Natural Science Foundation (ZR2011BQ017), the Research Project for the Application Foundation in Qingdao (13–4–198-jch), the National Key Technology Support Program (2012BAB15B02), and the National High-Tech Research and Development Programme of China (2010AA09Z203, 2010AA065104).

Supporting information for this article is available on the WWW under http://dx.doi.org/10.1002/anie.201409422.

effective excitation of N719 dyes, and we could thus establish a method to obtain DSSCs with maximum power conversion efficiency at a reduced cost and by a simplified process.

The crystal structures of the resultant CE materials were characterized by X-ray diffraction (XRD; Figure 1a). The characteristic diffraction peaks attributed to Co-Se [$Pa\bar{3}$ (No. 205), PDF: 88-1712], Ni-Se [$Pa\bar{3}$ (No. 205), PDF: 88-1711], Cu-Se [$P6_3/mmc$ (No. 194), PDF: 83-1814], Fe-Se [*Pmnn* (No. 58), PDF: 74-0247], and Ru-Se [$Pa\bar{3}$ (No. 205),

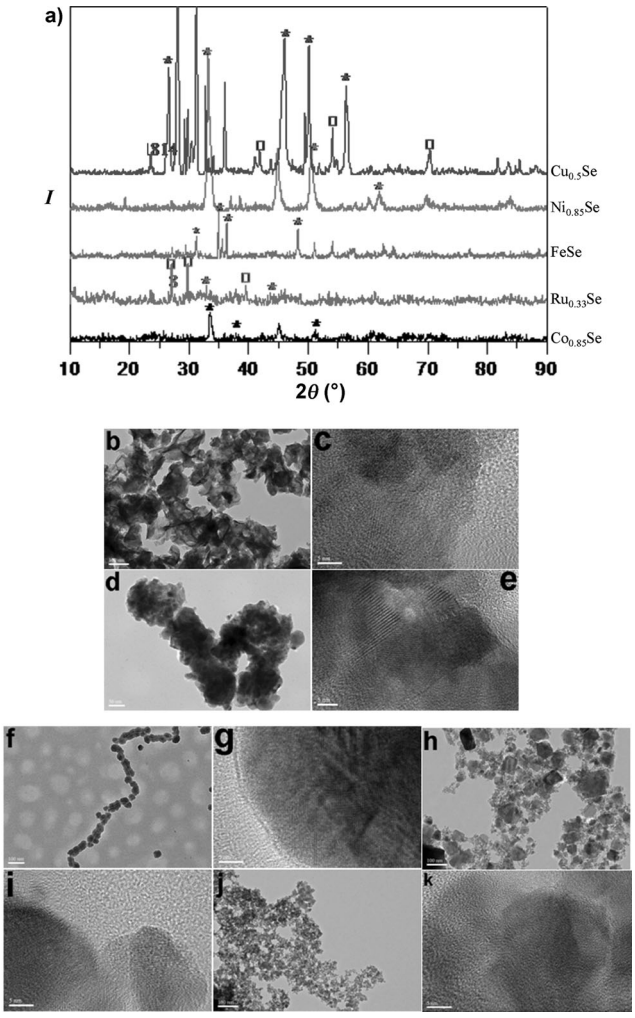

Figure 1. (a) XRD patterns and b–k) TEM photographs of the metal selenide alloys $Co_{0.85}Se$ (b, c), $Ni_{0.85}Se$ (d, e), $Cu_{0.50}Se$ (f, g), FeSe (h, i), and $Ru_{0.33}Se$ (j, k). The peaks denoted by * and □ are attributed to the metal selenide alloys and pure Se [*P*3121 (No. 152), PDF: 73-0465], respectively.

PDF: 03-1198] could be detected, indicating that the metal selenide alloys had been successfully synthesized by the mild solution strategy. The compositions of the as-synthesized metal selenide alloys were determined by inductively coupled plasma atomic emission spectroscopy (ICP-AES), giving atomic ratios of 0.858:1.000 ($Co_{0.85}Se$), 0.836:1.000 ($Ni_{0.85}Se$), 0.507:1.000 ($Cu_{0.50}Se$), 0.993:1.000 (FeSe), and 0.349:1.000 ($Ru_{0.33}Se$). The determined atomic ratios are close to their designated stoichiometries; therefore, the chemical formulae of the alloy CEs can be represented by the stoichiometric ratios. Low-resolution transmission electron microscopy (TEM) showed that the metal selenides have loose structures, which provide a large active surface for I_3^- diffusion and therefore accelerate the reduction reaction of $I_3^- \rightarrow I^-$. By high-resolution TEM, lattice fringes were clearly observed, indicating that the resultant metal selenide alloys have good crystallinities. Moreover, many lattice distortions were observed in their crystal lattices. These results indicate that the alloying of transition metals, such as Co, Ni, Cu, Fe, and Ru, with Se can feature abundant defects, which provide active sites for I_3^- adsorption and reduction.

To compare the optical transmission of the metal selenide alloy CEs with that of a Pt electrode, their transparencies were measured for light wavelengths of 400–1000 nm (Figure 2a). All of the alloy electrodes have a high optical transparency (>70%) in the visible and near-infrared regions, which is crucial for light penetration and dye excitation on rear irradiation. However, the transparency of a standard Pt electrode is only approximately 20% owing to the reflection of the incident light by its metallic surface. The pristine Pt cell exhibits modest front photocurrent–voltage (*J*–*V*) characteristics as a liquid DSSC under AM 1.5 irradiation; $V_{oc} = 0.712$ V (open-circuit voltage), $J_{sc} = 13.09\ mA\,cm^{-2}$ (short-circuit current density), FF = 66.3% (fill factor), and $\eta = 6.18\%$ (power conversion efficiency; Figure 2b). The optimal front η values for cells with $Co_{0.85}Se$, $Ni_{0.85}Se$, $Cu_{0.50}Se$, FeSe, and $Ru_{0.33}Se$ CEs are 8.30%, 7.85%, 6.43%, 7.64%, and 9.22%, respectively. Considering the high optical transparency (Figure 2c), the DSSCs based on alloy CEs have rear η values of 4.24–5.90%, which are higher than the value of 3.56% for the cell with a pristine Pt electrode. It is noteworthy that the J_{sc} and V_{oc} values are all lower for rear irradiation than for front irradiation. J_{sc} is a parameter that reflects the electron density in the conduction band of the TiO_2 nanocrystallite.[21] When the cell device is subjected to front irradiation, the incident light can penetrate the fluorine-doped tin oxide (FTO) glass substrate and excite the N719 dye, whereas it suffers from light loss across the FTO substrate, metal selenide alloy, and liquid electrolyte layers for rear irradiation. Therefore, the light intensity that is available for N719 irradiation, electron excitation, and therefore for promoting electrons into the conduction band of TiO_2 is higher for front irradiation than for rear irradiation. To describe the potential origin of the increased V_{oc} values for front irradiation, the path of the incident light and the electron density at the TiO_2 anode are illustrated in Figure S1. As the intensity of the incident light decreases within the TiO_2 film in a stepwise fashion, the amount of electrons generated by the excited dye is thus diminished. Therefore, the electron recombination with I_3^- species [$I_3^- + 2e_{CB}^-(TiO_2) \rightarrow 3I^-$] is retarded for front irradiation in comparison with rear irradiation. The maximum V_{oc} value is determined by the difference between the quasi-Fermi energy of the electrons in TiO_2 and the redox potential of the electrolyte,[22] whereas the real V_{oc} value of the DSSCs is smaller than this theoretical limit because of a backward reaction between photogenerated electrons and I_3^- species.[23] Therefore, the actual V_{oc} values obtained for front irradiation are higher than

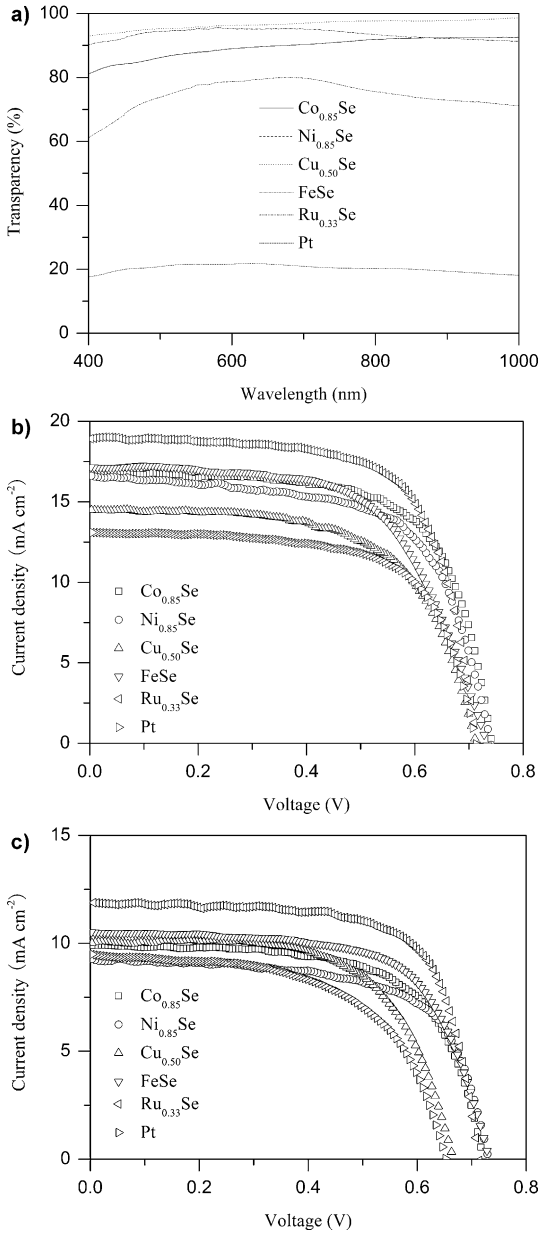

Figure 2. a) Optical transparency of various CEs. b, c) Characteristic *J–V* curves of their bifacial DSSCs for front (b) and rear (c) irradiation.

those for rear irradiation. The higher rear efficiency is attributed to the high optical transparency of the metal selenide CEs, which is solidly supported by the increased J_{sc} values. As references, the *J–V* curves of solar cells with pure metal electrodes have also been provided (Figure S2 and Table S1). Owing to the transition-metal nature of the Co, Ni, Cu, Fe, and Ru electrodes, they can be employed as CEs in DSSCs. More importantly, the alloying of such metals with selenium can markedly enhance the photovoltaic performance of DSSCs. Aside from metal selenide alloy electrodes, the mild solution strategy can also be employed to synthesize other cost-effective alloys, such as Pt-Mo and Pd-Co, to yield solar cells with a reasonable photovoltaic performance (Figure S3).

When evaluating the applicability of a CE it is very important to determine its catalytic activity towards the I_3^- reduction reaction.[24–26] As shown in Figure 3a, the cyclic voltammogram (CV) curves of various CEs in liquid electrolyte containing I^-/I_3^- redox couples have two pairs of redox peaks (Red_1: $I_3^- + 2e \rightarrow 3I^-/Ox_1$: $3I^- - 2e \rightarrow I_3^-$; Red_2: $3I_2 + 2e \rightarrow 2I_3^-/Ox_2$: $2I_3^- - 2e \rightarrow 3I_2$). The peak shapes and positions are similar to those observed with a standard Pt electrode, indicating that the metal selenide alloys have the same catalytic activities as Pt. Considering that the task of a CE is to reduce I_3^- ions to I^- species, the peak current intensity of Red_1 and the peak-to-peak separation (E_{pp}) between Red_1 and Ox_1 can be employed to evaluate the catalytic activity of the alloy electrodes.[27] The peak current density of Red_1 decreases in the following order: $Ru_{0.33}Se > Co_{0.85}Se > Ni_{0.85}Se > FeSe > Cu_{0.50}Se > Pt$. The E_{pp} of metal selenide alloy electrodes, a parameter negatively correlated with the standard electrochemical rate constant of a redox reaction, is approximately 110 mV, whereas it is 629.5 mV for the standard Pt electrode. The result indicates that the overpotential losses of alloy CEs are all lower than with a Pt electrode in DSSCs. Higher peak current densities and lower E_{pp} values suggest that the $Ni_{0.85}Se$ alloy electrode features a high catalytic activity in the reduction of I_3^- ions, which is a paramount prerequisite for a robust CE to be applied in a DSSC.[28,29] From the Bode electrochemical impedance spectroscopy (EIS) plots in Figure 3b, the actual lifetime (τ) of the electrons at the CE/electrolyte interface can be determined. The τ values are calculated according to $\tau = 1/2\pi f$,[30] where f is the peak frequency (Hz): $Ru_{0.33}Se$ (7.3 μs) < $Co_{0.85}Se$ (9.2 μs) < $Ni_{0.85}Se$ (19.2 μs) < FeSe (22.5 μs) < $Cu_{0.50}Se$ (31.9 μs) < Pt (75.2 μs). The reflux electrons (the electrons flowing from the external circuit to the CE) that are collected by the CE materials participate in the I_3^- reduction reaction ($I_3^- + 2e \rightarrow 3I^-$); therefore, a shorter electron lifetime implies a higher catalytic activity. Moreover, the $J_{ox1}/|J_{red1}|$ ratio is a parameter that can be used to determine the reversibility of the I^-/I_3^- redox reaction.[31] Values of 1.26, 1.27, 1.18, 1.06, and 1.24 were obtained for $Co_{0.85}Se$, $Ni_{0.85}Se$, $Cu_{0.50}Se$, FeSe, and $Ru_{0.33}Se$, respectively (1.39 for a standard Pt electrode), indicating that the $I_3^- \leftrightarrow I^-$ redox reaction is more reversible. For a real DSSC device, a higher reversibility implies the rapid conversion of I_3^- into I^- species for dye recovery. Therefore, more N719 molecules can excite electrons for electricity generation. Nyquist EIS was employed to confirm the catalytic behavior of various CEs (Figure 3c). The R_{ct} values were extracted by fitting the EIS plots using a Z-view software and summarized in Table 1. R_{ct} values increase in the order of $Ru_{0.33}Se$ (2.77 Ω cm^{-2}), $Co_{0.85}Se$ (2.84 Ω cm^{-2}), $Ni_{0.85}Se$ (2.96 Ω cm^{-2}), FeSe (4.90 Ω cm^{-2}), $Cu_{0.50}Se$ (5.44 Ω cm^{-2}), and Pt (7.23 Ω cm^{-2}), which is in good agreement with the CV and Bode EIS analysis. Tafel polarization curves for the symmetric dummy cells can be used to cross-check the catalytic activity of the electrodes (Figure 3d). Both the exchange current density (J_0) and the limiting diffusion current density (J_{lim}) decrease in the following order: $Ru_{0.33}Se > Co_{0.85}Se > Ni_{0.85}Se > FeSe > Cu_{0.50}Se > Pt$. J_0, obtained from the slopes for the anodic and cathodic branches, is inversely proportional to R_{ct}:[15] $J_0 = RT/nFR_{ct}$, where R is the gas constant, T

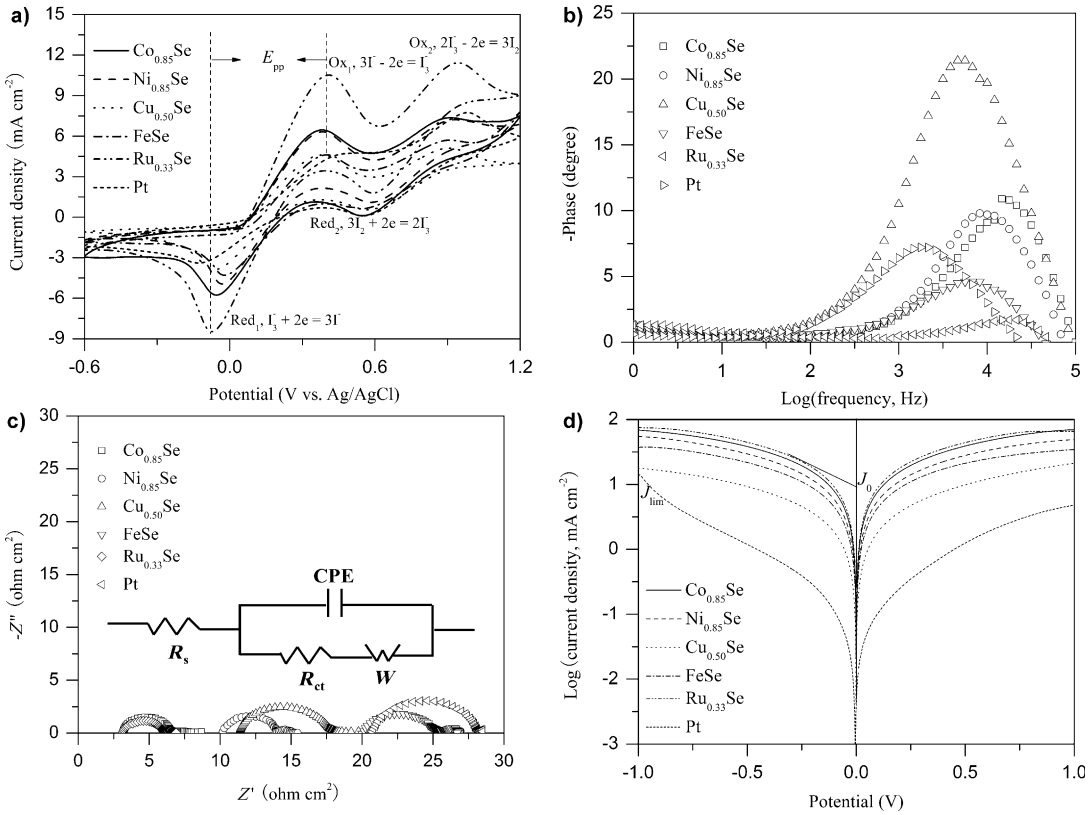

Figure 3. a) CV curves of various CEs for the I^-/I_3^- redox species recorded at a scan rate of 50 mV s^{-1}. b) Bode and c) Nyquist EIS plots and d) Tafel polarization curves of the symmetric dummy cells made from two identical CEs. The inset shows an equivalent circuit: CPE = constant phase element, R_{ct} = charge-transfer resistance, R_s = series resistance, W = Nernstian diffusion resistance.

Table 1: Photovoltaic parameters of DSSCs with various CEs and the simulated data from the EIS spectra.[a]

CEs	Irradiation	η [%]	V_{oc} [V]	FF [%]	J_{sc} [mA cm^{-2}]	R_{ct} [Ω cm^{-2}]
$Co_{0.85}Se$	front	8.30	0.742	66.8	16.74	2.84
	rear	4.63	0.721	64.7	9.92	
$Ni_{0.85}Se$	front	7.85	0.740	63.6	16.67	2.96
	rear	4.37	0.731	64.6	9.26	
$Cu_{0.50}Se$	front	6.43	0.713	62.0	14.55	5.44
	rear	4.24	0.666	63.6	10.01	
FeSe	front	7.64	0.733	61.0	17.10	4.90
	rear	5.05	0.732	65.8	10.49	
$Ru_{0.33}Se$	front	9.22	0.715	68.1	18.93	2.77
	rear	5.90	0.714	69.5	11.89	
Pt	front	6.18	0.712	66.3	13.09	7.23
	rear	3.56	0.652	57.6	9.48	

[a] FF: fill factor; J_{sc}: short-circuit current density, R_{ct}: charge-transfer resistance; V_{oc}: open-circuit voltage; η: power conversion efficiency.

the absolute temperature, and F is Faraday's constant. Apparently, the calculated R_{ct} values match the order determined by EIS and CV analysis. Furthermore, J_{lim}, a parameter that depends on the diffusion coefficient (D_n) of the I^-/I_3^- redox couple at the CE/electrolyte interface, is proportional to D_n:[32] $J_{lim} = 2nFCD_n/l$, where l is the distance between the electrodes in a dummy cell, n is the number of electrons involved in the reduction of I_3^-, and C is the I_3^- concentration. D_n can also be obtained by the Randles–Sevcik theory:[33] $J_{red} = Kn^{1.5}ACD_n^{0.5}v^{0.5}$, where J_{red} is the peak current density of Red_1, K is 2.69×10^5, A is the active area of the dummy cell, and v is the scan rate for the CV curves. The calculated D_n values that are shown in Figure 3a are in decreasing order: 9.90×10^{-7} cm^{-2}s^{-1} ($Ru_{0.33}Se$), 4.59×10^{-7} cm^{-2}s^{-1} ($Co_{0.85}Se$), 3.38×10^{-7} cm^{-2}s^{-1} ($Ni_{0.85}Se$), 2.62×10^{-7} cm^{-2}s^{-1} (FeSe), $2.09 \times \times 10^{-7}$ cm^{-2}s^{-1} ($Cu_{0.50}Se$), and 1.67×10^{-7} cm^{-2}s^{-1} (Pt). At this point, we can therefore conclude that the results from CV, Bode EIS, Nyquist EIS, and Tafel measurements are in good agreement.

To be applied as windows, roof panels, or portable sources, solar panels should feature several crucial characteristics, including start-up behavior, multiple start/stop capability, and photocurrent stability.[34] For realizing these objectives, we measured the start/stop switching by alternatively illuminating and darkening the DSSCs with metal selenide electrodes for irradiation at the front, rear, and both (Figure 4a; see also Figure S4). The related performance of the platinum-based cell device were also recorded as a reference. There is an abrupt increase in photocurrent density on irradiation from the front, rear, or both, suggesting that the solar cell has been started, whereas no delay in starting the cell demonstrates that the $Ru_{0.33}Se$ alloy electrode is vigorous in transferring electrons and catalyzing I_3^- reduction. In each "start" state, no obvious attenuation in photocurrent density was observed for the cells with the $Ru_{0.33}Se$, $Co_{0.85}Se$, $Ni_{0.85}Se$, and FeSe electrodes. This phenomenon is a sign of low electron recombination with I_3^-,[35] which is in an agreement with the J–V curves measured in the dark (Figure S5). However, with

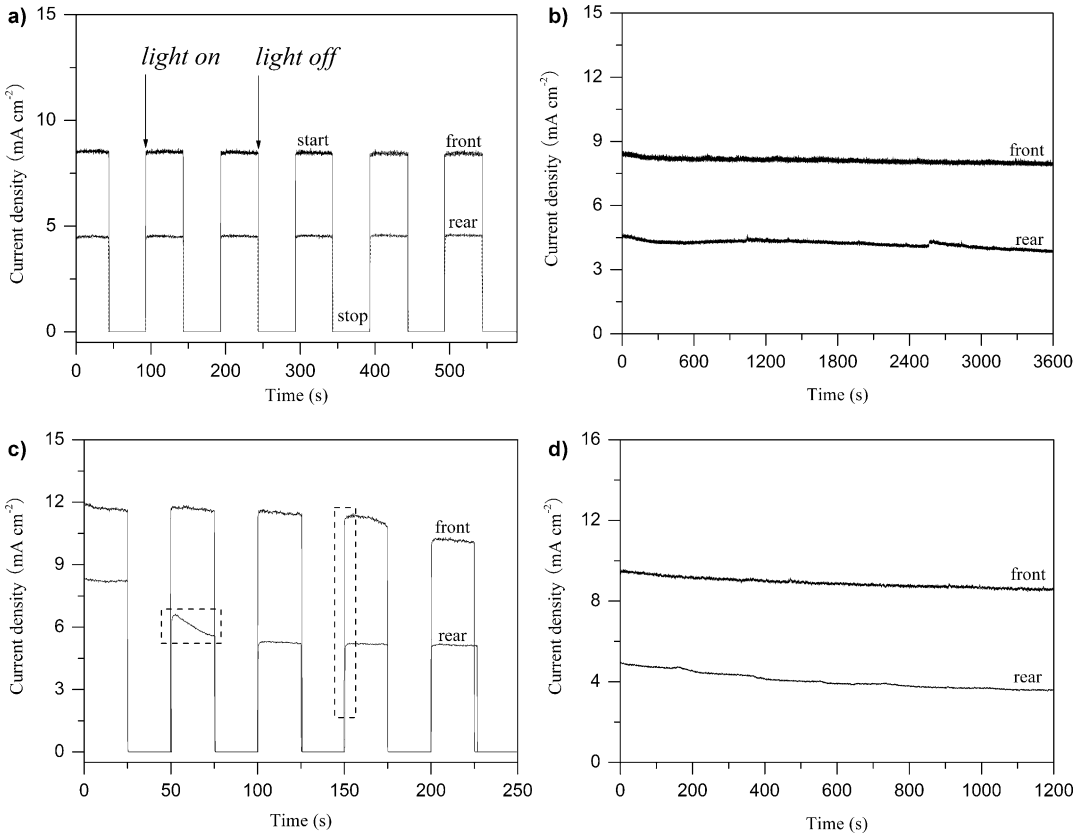

Figure 4. a, c) Start/stop switching by alternatively irradiating (100 mW cm^{-2}) and darkening (0 mW cm^{-2}) a cell device with a $Ru_{0.33}Se$ (a) or a Pt electrode (c) at an interval of 25 s and at 0 V. b, d) Photocurrent stabilities under continuous irradiation at 100 mW cm^{-2} for cell devices with $Ru_{0.33}Se$ (b) and Pt electrodes (d).

the standard Pt electrode, a delay in the start of the activity of the DSSC was observed, which is due to a lower activity in reducing I_3^- ions, whereas the high dark current density leads to an apparent attenuation in photocurrent. Furthermore, the alternation of day and night leads to multiple start/stop cycles. Therefore, an efficient solar cell should feature a good start/stop capability. In comparison with the standard Pt electrode, the cell with $Ru_{0.33}Se$ still has fast start-up characteristics and a stable photocurrent density after several start/stop cycles. A remaining issue in obtaining a robust DSSC is the photovoltaic stability under continuous irradiation. As shown in Figure 4b, 97.4% and 86.7% of the initial photocurrent densities were maintained after one hour of operation for front and rear irradiation, respectively; however, for the DSSC with the standard Pt electrode, they had decreased to 89.6% and 72.3% of the initial values after only 20 minutes. The comparison suggests a relatively good stability for the cell employing the $Ru_{0.33}Se$ alloy electrode. Moreover, the photocurrent stabilities of the $Co_{0.85}Se$ and $Ni_{0.85}Se$ based cells are also modest.

In summary, we have demonstrated that the mild solution-based synthesis of transparent M-Se (M = Co, Ni, Cu, Fe, Ru) binary alloys is an effective strategy for obtaining cost-effective CE materials and enhancing the photovoltaic performance of DSSCs. All of the metal selenide alloys feature superior electrocatalytic activities towards I_3^- reduction and a higher charge-transfer ability than the standard Pt electrode. The bifacial DSSCs with $Co_{0.85}Se$, $Ni_{0.85}Se$, $Cu_{0.50}Se$, FeSe, and $Ru_{0.33}Se$ alloy electrodes display impressive power conversion efficiencies of 8.30, 7.85, 6.43, 7.64, and 9.22% for front irradiation, and 4.63, 4.37, 4.24, 5.05, and 5.90% for rear irradiation, respectively. The measured efficiencies are much higher than the 6.18% and 3.56% obtained for the solar cell with the pristine Pt electrode on front and rear irradiation. Significant features of these electrodes, including fast activity onset, multiple start/stop capability, and modest photocurrent stability, should motivate their use in bifacial DSSCs employed as windows, roof panels, or portable energy sources. The DSSCs presented herein are far from being fully optimized, but these profound advantages along with the cost-effective and scalable synthesis suggest that the new transparent alloy CEs are strong candidates for bifacial DSSCs. Moreover, the high optical transparency and the charge-transfer ability should enable the application of the transparent metal selenide alloys as back electrodes in bifacial perovskite solar cells.

Received: September 23, 2014
Revised: October 15, 2014
Published online: October 30, 2014

Keywords: alloys · electrocatalysis · energy conversion · metal selenides · solar cells

[1] X. X. Chen, Q. W. Tang, B. L. He, L. Lin, L. M. Yu, *Angew. Chem. Int. Ed.* **2014**, *53*, 10799 – 10803; *Angew. Chem.* **2014**, *126*, 10975 – 10979.
[2] Y. Luo, D. Li, Q. B. Meng, *Adv. Mater.* **2009**, *21*, 4647 – 4651.
[3] M. Kimura, H. Nomoto, N. Masaki, S. Mori, *Angew. Chem. Int. Ed.* **2012**, *51*, 4371 – 4374; *Angew. Chem.* **2012**, *124*, 4447 – 4450.
[4] I. Chung, B. Lee, J. Q. He, R. P. H. Chang, M. G. Kanatzidis, *Nature* **2012**, *485*, 486 – 489.
[5] B. O'Regan, M. Grätzel, *Nature* **1991**, *353*, 737 – 740.
[6] A. Yella, H. W. Lee, H. N. Tsao, C. Yi, A. K. Chandiran, M. K. Nazeeruddin, E. W. G. Diau, C. Y. Yeh, S. M. Zakeeruddin, M. Grätzel, *Science* **2011**, *334*, 629 – 634.
[7] E. J. W. Crossland, N. Noel, V. Sivaram, T. Leijtens, J. A. Webber, H. J. Snaith, *Nature* **2013**, *495*, 215 – 219.
[8] M. Liang, J. Chen, *Chem. Soc. Rev.* **2013**, *42*, 3453 – 3488.
[9] Y. Y. Duan, Q. W. Tang, Z. H. Chen, B. L. He, H. Y. Chen, *J. Mater. Chem. A* **2014**, *2*, 12459 – 12465.
[10] S. F. Zhang, X. D. Yang, Y. Numata, L. Y. Han, *Energy Environ. Sci.* **2013**, *6*, 1443 – 1464.
[11] Y. Xue, J. Liu, H. Chen, R. Wang, D. Li, J. Qu, L. M. Dai, *Angew. Chem. Int. Ed.* **2012**, *51*, 12124 – 12127; *Angew. Chem.* **2012**, *124*, 12290 – 12293.
[12] D. W. Chang, H. J. Choi, A. Filer, J. B. Baek, *J. Mater. Chem. A* **2014**, *2*, 12136 – 12149.
[13] Q. W. Tang, H. Y. Cai, S. S. Yuan, X. Wang, *J. Mater. Chem. A* **2013**, *1*, 317 – 323.
[14] B. L. He, Q. W. Tang, T. L. Liang, Q. H. Li, *J. Mater. Chem. A* **2014**, *2*, 3119 – 3126.
[15] F. Gong, H. Wang, X. Xu, G. Zhou, Z. S. Wang, *J. Am. Chem. Soc.* **2012**, *134*, 10953 – 10958.
[16] X. Xin, M. He, W. Han, J. Jung, Z. Q. Lin, *Angew. Chem. Int. Ed.* **2011**, *50*, 11739 – 11742; *Angew. Chem.* **2011**, *123*, 11943 – 11946.
[17] M. X. Wu, X. Lin, Y. D. Wang, L. Wang, W. Guo, D. D. Qi, X. J. Peng, A. Hagfeldt, M. Grätzel, T. L. Ma, *J. Am. Chem. Soc.* **2012**, *134*, 3419 – 3428.
[18] S. Ito, S. M. Zakeeruddin, P. Comte, P. Liska, D. Kuang, M. Grätzel, *Nat. Photonics* **2008**, *2*, 693 – 698.
[19] J. Bisquert, *Nat. Photonics* **2008**, *2*, 648 – 649.
[20] Q. D. Tai, B. Chen, F. Guo, S. Xu, H. Hu, B. Sebo, X. Z. Zhao, *ACS Nano* **2011**, *5*, 3795 – 3799.
[21] W. Shao, F. Gu, C. Z. Li, M. K. Lu, *Ind. Eng. Chem. Res.* **2010**, *49*, 9111 – 9116.
[22] D. Cahen, G. Hodes, M. Gätzel, J. F. Guillemoles, I. Riess, *J. Phys. Chem. B* **2000**, *104*, 2053 – 2059.
[23] H. S. Jung, J. K. Lee, *J. Phys. Chem. Lett.* **2013**, *4*, 1682 – 1693.
[24] W. C. Liu, Y. Liu, J. R. Jennings, H. Huang, Q. Wang, *J. Mater. Chem. A* **2014**, *2*, 10938 – 10944.
[25] R. Trevisan, M. Döbbelin, P. P. Boix, E. M. Barea, R. Tena-Zaera, I. Mora-Seró, J. Bisquert, *Adv. Energy Mater.* **2011**, *1*, 781 – 784.
[26] G. R. Li, F. Wang, Q. W. Jiang, X. P. Gao, P. W. Shen, *Angew. Chem. Int. Ed.* **2010**, *49*, 3653 – 3656; *Angew. Chem.* **2010**, *122*, 3735 – 3738.
[27] J. Liu, Q. W. Tang, B. L. He, *J. Power Sources* **2014**, *268*, 56 – 62.
[28] X. Zheng, J. Deng, N. Wang, D. Deng, W. H. Zhang, X. H. Bao, C. Li, *Angew. Chem. Int. Ed.* **2014**, *53*, 7023 – 7027; *Angew. Chem.* **2014**, *126*, 7143 – 7147.
[29] H. Y. Cai, Q. W. Tang, B. L. He, P. J. Li, *J. Power Sources* **2014**, *258*, 117 – 121.
[30] J. Yoon, M. Jin, M. Lee, *Adv. Mater.* **2011**, *23*, 3974 – 3978.
[31] H. Tributsch, *Coord. Chem. Rev.* **2004**, *248*, 1511 – 1530.
[32] M. K. Wang, A. M. Anghel, B. Marsan, N. C. Ha, N. Pootrakulchote, S. M. Zakeeruddin, M. Grätzel, *J. Am. Chem. Soc.* **2009**, *131*, 15976 – 15977.
[33] M. J. Ju, I. Y. Jeon, J. C. Kim, K. Lim, H. J. Choi, S. M. Jung, I. T. Choi, Y. K. Eom, Y. J. Kwon, J. Ko, J. J. Lee, H. K. Kim, J. B. Baek, *Adv. Mater.* **2014**, *26*, 3055 – 3062.
[34] C. Laberty-Robert, K. Vallé, F. Pereira, C. Sanchez, *Chem. Soc. Rev.* **2011**, *40*, 961 – 1005.
[35] Z. Y. Tang, J. H. Wu, M. Zheng, J. H. Huo, Z. Lan, *Nano Energy* **2013**, *2*, 622 – 627.

